BULLETIN OF THE POLISH ACADEMY OF SCIENCES
TECHNICAL SCIENCES, Vol. 70(4), 2022, Article number: e141722
DOI: 10.24425/bpasts.2022.141722

Dynamic characteristics of underframe semi-active inerter-based suspended device for high-speed train based on LQR control

Yong WANG[1,2]*, Hao-Xuan LI[2], Hao-Dong MENG[3], and Yang WANG[1]**

[1] State Key Laboratory of Automotive Simulation and Control, Jilin University, Changchun 130022, China
[2] Automotive Engineering Research Institute, Jiangsu University, Zhenjiang 212013, China
[3] School of Automotive Engineering, Changzhou Institute of Technology, Changzhou 213002, China

Abstract. The underframe passive inerter-based suspended device, based on the inerter-spring-damper vibration attenuation structure, could improve the dynamic performance of the train body, but its parameters are fixed and cannot meet the dynamic performance requirements under different operating conditions. Therefore, a semi-active inerter-based suspended device based on the linear quadratic regulator (LQR) control strategy is proposed to further enhance the dynamic performance. The rigid-flexible coupling vertical dynamic model of the train body and an underframe semi-active inerter-based suspended device are established. The structural parameters of the semi-active inerter-based suspended device are adjusted using LQR control strategy. Dynamic response of the system is obtained using the virtual excitation method. The dynamic characteristic of the system is evaluated using the Sperling index and compared with those of the passive and semi-active traditional suspended devices as well as the passive inerter-based suspended devices. The vertical vibration acceleration of the train body and Sperling index using the semi-active inerter-based suspended device is the smallest among the four suspended devices, which denotes the advantages of using the inerter and LQR control strategy. The semi-active inerter-based suspended device could decrease the vertical vibration acceleration of the train body and further suppress its elastic vibration in the lower frequency band, more effectively than the other three suspended devices. Overall, the semi-active inerter-based suspended device could significantly reduce elastic vibration of the train body and improve its dynamical performance.

Key words: dynamic characteristic, high-speed train, inerter-based suspended device, LQR control, Sperling index.

1. INTRODUCTION

As major breakthroughs have been made in many key areas of the high-speed train industry, the trains' operating speed increases gradually. Safety, comfort and speed are the fundamental goals of high-speed trains [1], as a railway transportation system with faster running speed, better travel comfort and higher safety are all urgently required. In order to achieve this goal, the lightweight design criterion and power decentralized traction are normally used in high-speed trains [2]. Lightweight design reduces the weight of high-speed train components and increases operating speed. However, rigidity of the train is reduced, which aggravates the elastic vibration of the train body and further deteriorates the travel comfort [3, 4]. The power decentralized traction needs to have the suspended device installed under the train body, which reduces axle load and the wear of wheels and rails, while also improving service time and dynamic performance. However, coupled vibration between the train body and underframe suspended device then occurs [5].

Many scholars have studied the dynamic characteristic of the train body and underframe suspended device. Tomioka *et al.* [6] investigated interaction between the train body and longitudinal bogie, and regarded the longitudinal bogie as a dynamic vibration absorber (DVA), which effectively reduces vibration of the train body. Gong *et al.* [7] established the rigid-flexible coupling vertical dynamic model of the train body and underframe suspended device, calculated its natural frequencies and found that coupling vibration could be suppressed through adjusting suspension stiffness. Yang *et al.* [8] proposed a train model considering the roll motion of the train body, established a three-dimensional multi-body dynamic model in SIMPACK and found that coupling vibration would be reduced via increasing the roll moment inertia of the system. In the above research studies, the suspended device is based on the spring-damper vibration attenuation structure, but further improvement of the running smoothness and travel comfort of the high-speed train is restricted by the inherent structure of the traditional suspended device. Therefore, a new vibration attenuation structure should be sought to enhance dynamic performance.

In 2002, Smith [9] proposed the concept of an inerter, which is a device with two freely moving terminals, and its generated force is proportional to relative acceleration. This proportional constant is denoted as inertance and measured in kilograms. As a new type of vibration attenuation device, the inerter has been widely used in many areas and shown its advantages *inter alia* in vehicle suspension systems [10–12], aircraft landing gears [13], seismic mitigation systems [14, 15],

*e-mail: wangy1921@126.com
**e-mail: yangwang@jlu.edu.cn

Manuscript submitted 2022-01-26, revised 2022-05-16, initially accepted for publication 2022-05-25, published in August 2022.

dynamic vibration absorption structures [16] and vibration isolation systems [17–19]. At present, the application of an inerter used in a high-speed train has attracted the attention of related scholars. Jiang *et al.* [20] proposed a 7 degree-of-freedom (DOF) half train body model and investigated several inerter-based suspension layouts, which shows that reasonable suspension layout could improve the lateral and vertical travel comfort. Chen *et al.* [21] proposed a 31 DOF train model with inerter-based suspension, and applied network synthesis methods to construct the inerter-based structures, which effectively enhances dynamic performance and running stability. Lewis *et al.* [22] proposed a 6 DOF train model using both Hall-Bush longitudinal and inerter-based lateral suspensions, and found that using an inerter in lateral suspension could reduce track wear and enhance the travel comfort. In the above mentioned studies, the inerter is used in the secondary suspension system of a high-speed train, while the inerter utilized in the underframe suspended device has rarely been investigated.

Wang *et al.* [23] firstly applied the inerter in the underframe suspended device for a high speed train, established the rigid-flexible coupling vertical dynamic model of the train body and inerter-based suspended device, studied the dynamic characteristic of the coupled system and evaluated the dynamic performance using the Sperling index. The results showed that the inerter-based suspended device could effectively attenuate vibration of the train body and improve the dynamic performance more effectively than the traditional suspended device. For the passive inerter-based suspended device, the structural parameters are fixed and cannot satisfy the dynamic performance requirements under different operating conditions. Active and semi-active control strategies are the way to further reduce vibration of the train body and further improve its dynamic performance. Active control strategies, including PID control [24], model predict control [25] and active disturbance rejection control [26, 27], are commonly used control strategies. Semi-active control strategies, including optimal control [28,29], sliding mode control [30, 31], fuzzy control [32] and robust control [33], are also commonly used control strategies. Compared with active control structure, semi-active control structure has the advantages of simple form and low energy consumption. Therefore, the semi-active inerter-based suspended device is proposed, based on the semi-active inerter, semi-active damper and passive spring. The main goal is to investigate how the semi-active inerter-based suspended device influences the dynamic response and further enhances dynamic performance.

Optimal control strategies, including H_2 optimal control [34], H_∞ optimal control [35] and optimal preview control [36, 37], are mostly studied for high-speed trains. The H_2 optimal control strategy can be transformed into an optimal feedback system using linear state feedback control, which could be easily implemented in practical engineering. The linear quadratic regulator (LQR) control strategy is a type of H_2 optimal control which has a very practical and clear physical meaning. Design of the control system is more standardized, has a unified analytical form, and manifests strong comprehensiveness and applicability. The linear quadratic Gaussian (LQG) control strategy minimizes the quadratic performance index for stochastic linear systems with Gaussian noise, while for the high-speed train, the typical track spectrum is not the Gaussian noise, so the LQR control strategy is used for the semi-active inerter-based suspended device in this paper, which regulates the inertance of the semi-active inerter and the damping of the semi-active damper. The main novelty of this paper is the following: (a) A semi-active inerter-based suspended device based on the LQR control strategy is proposed. (b) The rigid-flexible coupling vertical dynamic model of the train body and underframe semi-active inerter-based suspended device is established. (c) The effect of the semi-active inerter-based suspended device on the dynamic performance of the coupling dynamic system is studied and compared with those of the passive one to show its advantages.

The structure of the paper is as follows: in Section 2, the passive inerter-based suspended device is constructed and the rigid-flexible coupling vertical dynamic model of the train body and underframe suspended device is established. In Section 3, the semi-active inerter-based suspended device based on LQR control is proposed. In Section 4, the dynamic performance of the coupling dynamic system is studied. Overall conclusions are presented in Section 5.

2. PASSIVE INERTER-BASED SUSPENDED DEVICE AND ITS MODELING

In order to accurately describe the elastic vibration of the train body, the train body can be considered as a Euler–Bernoulli beam or a Timoshenko beam. The Euler–Bernoulli beam model considers the bending deformation of the train body without considering its shear deformation. The Timoshenko beam model considers the shear deformation and rotational inertia of the train body, so this model is more accurate and the frequency range for calculation and analysis is wider. Bearing in mind that the vibration frequency range of the conventional train is generally within 50 Hz, in this medium and low frequency range, the analysis results of the Euler–Bernoulli beam and Timoshenko beam models show little difference [4, 7]. In addition, theoretical analysis of the Timoshenko beam model is more complex. From the perspective of engineering application, the Euler–Bernoulli beam model can also accurately reflect the actual elastic vibration of the train body. In view of this, the elastic train body is equivalent to the Euler–Bernoulli beam with equal section and the underframe suspended device is installed under the middle of the train body, which can accurately describe the coupling vibration of the elastic train body and underframe suspended device. Therefore, the rigid-flexible coupling vertical dynamic model of the train body and inerter-based suspended device is established and shown in Fig. 1. It is composed of the train body, bogie, wheel set, primary and secondary suspension systems, and an underframe inerter-based suspended device. The inerter-based suspended device is based on the inerter-spring-damper vibration attenuation structure. To facilitate research, the bogie, wheel set and suspended device are regarded as rigid bodies. The coupling dynamic model has 9 DOF. The underframe suspended device has a bouncing DOF. Each bogie has a bouncing DOF and a pitching DOF, respectively. The train body also has a bouncing DOF and a pitching

DOF, respectively, and, in addition, the first two vertical elastic modes of the train body are considered. The total length of the train body is L, vertical and pitching displacements of the train body are $z(x,t)$ and θ_b, respectively, vertical and pitching displacements of bogie 1 (left) and bogie 2 (right) are z_1, z_2, θ_1 and θ_2, respectively, while vertical displacement of the underframe suspended device is z_3. The wheel pairs are set close to the rails whose displacement is the input track irregularity, and the vertical excitations of the track irregularity of the four wheel sets are $z_{\omega 1}$, $z_{\omega 2}$, $z_{\omega 3}$ and $z_{\omega 4}$, respectively. The structural parameters of the coupling dynamic model are listed in Table 1.

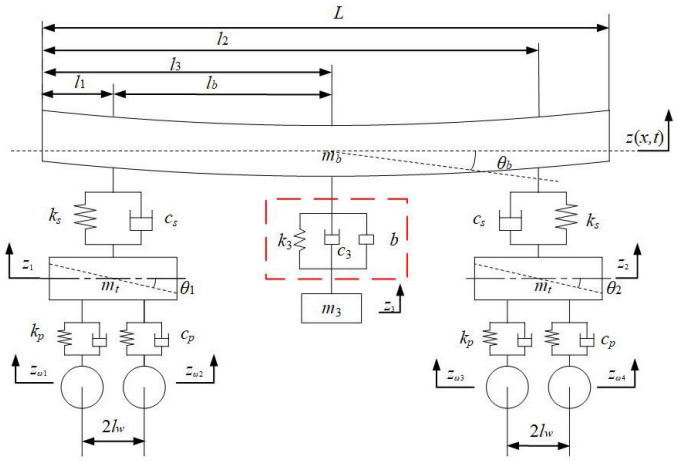

Fig. 1. Rigid-flexible coupling vertical dynamic model of the train body and underframe inerter-based suspended device

Table 1
Structural parameters of the coupling dynamic model

Parameter	Symbol	Value	Unit
Mass of train	m_b	29	t
Train body pitch inertia	I_b	1420	t·m^2
Mass of bogie	m_t	2200	t
Bogie pitch inertia	I_t	1200	kg·m^2
Secondary spring stiffness per bogie	k_s	260	kN/m
Secondary damping per bogie	c_s	20	kN·s/m
Primary spring stiffness per bogie	k_p	2000	kN/m
Primary damping per bogie	c_p	20	kN·s/m
Half of bogie center	l_b	8.75	m
Half of wheel base	l_w	1.25	m
Train body length	L	24.5	m
First bending frequency	ω_3	$12.3\times 2\pi$	rad/s
First bending damping ratio	ξ_3	1.5	%
Second bending frequency	ω_4	$17\times 2\pi$	rad/s
Second bending damping ratio	ξ_4	1.5	%
Mass of suspended device	m_3	4500	kg

The train body is simplified as the Euler–Bernoulli beam with equal cross-section [38], and its vibration equation is given as:

$$\ddot{q}_i(t)+2\xi_i\omega_i\dot{q}_i(t)+\omega_i^2 q_i(t) = \frac{Y_i(l_1)}{m_b}P_1+\frac{Y_i(l_2)}{m_b}P_2+\frac{Y_i(l_3)}{m_b}P_3;\quad i=3,4,\ldots,n, \tag{1}$$

$$Y_i(x)=\mathrm{ch}\beta_i x+\cos\beta_i x-\frac{\mathrm{ch}\lambda_i-\cos\lambda_i}{\mathrm{sh}\lambda_i-\sin\lambda_i}(\mathrm{sh}\beta_i+\sin\beta_i), \tag{2}$$

$$l_1=\frac{L}{2}-l_b,\quad l_2=\frac{L}{2}+l_b,\quad l_3=\frac{L}{2}, \tag{3}$$

$$1-\mathrm{ch}\lambda_i\cos\lambda_i=0, \tag{4}$$

$$\beta_i=\lambda_i/L, \tag{5}$$

$$\lambda_i=(2i+1)\pi/2, \tag{6}$$

where ω_i, ξ_i, $Y_i(x)$ and $q_i(t)$ are the natural frequency, damping ratio, mode function and mode coordinate of the ith-order elastic mode for the train body, respectively. l_1 and l_2 are the distances from the center of the secondary suspension system of bogie 1 (left) and bogie 2 (right) to the left end of the train body, respectively, and l_3 is the distance from the center of the underframe suspended device to the left end of the train body, which is also shown in Fig. 1. Based on equations (1), (2), (3), (4), (5) and (6), the vibration equation and the first two vertical elastic modes of the train body can be determined.

P_1, P_2 and P_3 are the forces of the primary suspension, secondary suspension and inerter-based suspended device acting on the train body, respectively. The three forces are expressed as:

$$\begin{cases} P_1=-k_s[z(l_1,t)-z_1]-c_s[z'(l_1,t)-z_1'], \\ P_2=-k_s[z(l_2,t)-z_2]-c_s[z'(l_2,t)-z_2'], \\ P_3=-k_3[z(l_3,t)-z_3]-c_3[z'(l_3,t)-z_3'] \\ \qquad -b[z''(l_3,t)-z_3'']. \end{cases} \tag{7}$$

According to Fig. 1, the vertical and torsional dynamic equations of the train body are established as:

$$m_b z_b''=P_1+P_2+P_3, \tag{8}$$

$$I_b\theta_b''(t)=P_1\left(\frac{L}{2}-l_1\right)+P_2\left(\frac{L}{2}-l_2\right)+P_3\left(\frac{L}{2}-l_3\right). \tag{9}$$

Bearing in mind that the first two modes of the train body are rigid modes, the first and second elastic modes are mainly considered in this paper, which are expressed as q_3 and q_4, and the corresponding dynamic equations are given as:

$$q_3''(t)+2\xi_3\omega_3 q_3'(t)+\omega_3^2 q_3(t) = \frac{Y_3(l_1)}{m_b}P_1+\frac{Y_3(l_2)}{m_b}P_2+\frac{Y_3(l_3)}{m_b}P_3, \tag{10}$$

$$q_4''(t)+2\xi_4\omega_4 q_4'(t)+\omega_4^2 q_4(t) = \frac{Y_4(l_1)}{m_b}P_1+\frac{Y_4(l_2)}{m_b}P_2+\frac{Y_4(l_3)}{m_b}P_3\,. \tag{11}$$

The vertical and torsional dynamic equations of the left bogie are given by:

$$m_t z_1''+c_p(2z_1'-z_{\omega1}'-z_{\omega2}') +k_p(2z_1-z_{\omega1}-z_{\omega2})=-P_1\,, \tag{12}$$

$$I_t\theta_1''+2l_w^2c_p\theta_1'+2l_w^2k_p\theta_1 =-l_wc_pz_{\omega1}'+l_wc_pz_{\omega2}'-l_wk_pz_{\omega1}+l_wk_pz_{\omega2}\,. \tag{13}$$

The vertical and torsional dynamic equations of the right bogie are given by:

$$m_t z_2''+c_p(2z_2'-z_{\omega3}'-z_{\omega4}') +k_p(2z_2-z_{\omega3}-z_{\omega4})=-P_2\,, \tag{14}$$

$$I_t\theta_2''+2l_w^2c_p\theta_2'+2l_w^2k_p\theta_2 =-l_wc_pz_{\omega3}'+l_wc_pz_{\omega4}'-l_wk_pz_{\omega3}+l_wk_pz_{\omega4}\,. \tag{15}$$

The vertical dynamic equation of the underframe suspended device is given as:

$$m_3z_3''-k_3[z(l_3,t)-z_3] -c_3[z'(l_3,t)-z_3']-b[z''(l_3,t)-z_3'']=0. \tag{16}$$

Using equation (7), equations (8), (9), (10), (11), (12), (13), (14), (15), and (16) can be written in a matrix form

$$\begin{aligned}\mathbf{MZ}''+\mathbf{CZ}'+\mathbf{K}_1\mathbf{Z}&=\mathbf{DZ}_\omega\,,\\ \mathbf{Z}&=[z_b\theta_bq_3q_4z_1\theta_1z_2\theta_2z_3]^T,\\ \mathbf{Z}_\omega&=[z_{\omega1}z_{\omega1}'z_{\omega2}z_{\omega2}'z_{\omega3}z_{\omega3}'z_{\omega4}z_{\omega4}']^T,\end{aligned} \tag{17}$$

where $\mathbf{M}$ is the mass matrix, $\mathbf{C}$ is the damping matrix, $\mathbf{K}_1$ is the stiffness matrix and $\mathbf{D}$ is the input excitation matrix, with the definitions of these matrices being given in the Appendix.

As the high-speed train runs on a fixed track, the input of the second, third and fourth wheel sets could be treated as the delay of the first wheel set. Assuming that there exists no time delay in the roughness input for the first wheel set and with its self-density being $S_{FF}(\omega)$, the corresponding virtual excitation is:

$$\begin{aligned}\mathbf{Z}_\omega&=\begin{bmatrix}z_{\omega1}(t)\\ z_{\omega2}(t)\\ z_{\omega3}(t)\\ z_{\omega4}(t)\end{bmatrix}=\begin{bmatrix}z_{\omega1}(t)\\ z_{\omega1}(t-\tau_1)\\ z_{\omega1}(t-\tau_2)\\ z_{\omega1}(t-\tau_3)\end{bmatrix}=\begin{bmatrix}1\\ e^{-j\omega\tau_1}\\ e^{-j\omega\tau_2}\\ e^{-j\omega\tau_3}\end{bmatrix}z_{\omega1}(t)\\ &=\begin{bmatrix}1\\ e^{-j\omega\tau_1}\\ e^{-j\omega\tau_2}\\ e^{-j\omega\tau_3}\end{bmatrix}\sqrt{S_{FF}(\omega)}e^{i\omega t},\end{aligned} \tag{18}$$

where $\tau_1=2l_w/v$, $\tau_2=2l_b/v$ and $\tau_3=2(l_w+l_b)/v$. As the track spectrum is determined and taken as the input excitation, self-density $S_{FF}(\omega)$ for the first wheel set roughness input can be obtained, and combining equations (18) and (A4), the input excitation $\mathbf{DZ}_\omega$ in equation (17) can be determined.

Substituting equation (18) into equation (17) yields the following:

$$\mathbf{H}(\omega)=[-\omega^2\mathbf{M}+\omega\mathbf{C}+\mathbf{K}]^{-1}\mathbf{D}\begin{bmatrix}1\\ e^{-j\omega\tau_1}\\ e^{-j\omega\tau_2}\\ e^{-j\omega\tau_3}\end{bmatrix}z_{\omega1}(t), \tag{19}$$

$$\mathbf{Y}=[-\omega^2\mathbf{M}+\omega\mathbf{C}+\mathbf{K}]^{-1}\mathbf{D}\begin{bmatrix}1\\ e^{-j\omega\tau_1}\\ e^{-j\omega\tau_2}\\ e^{-j\omega\tau_3}\end{bmatrix}. \tag{20}$$

Then the dynamic response power spectrum is:

$$S_{yy}=\mathbf{H}(\omega)^*\mathbf{H}(\omega)^T=\mathbf{Y}^*\mathbf{Y}^T, \tag{21}$$

where $\mathbf{Y}^*$ and $\mathbf{Y}^T$ are the conjugate and transpose vectors of $\mathbf{Y}$, respectively. Based on equation (21), the amplitude at each sampling frequency could be solved as:

$$a_k^2=4S_{yy}(\omega_k)\Delta\omega, \tag{22}$$

where $\Delta\omega=(\omega_\mu-\omega_l)/N$ is the sampling frequency interval, $\omega_\mu=200\pi$ and $\omega_l=0.6\pi$ are the upper and lower cut-off frequencies, and $N=2500$ stands for the sampling points.

Therefore, the dynamic response power spectrum S_{yy} can be obtained using the virtual excitation method. There exists no time domain or frequency domain integration in the solving process, which greatly simplifies the calculation.

3. SEMI-ACTIVE INERTER-BASED SUSPENDED DEVICE AND ITS MODELING

Then, the semi-active inerter-based suspended device is constructed. The semi-active inerter-based suspended device is based on the semi-active inerter and semi-active damper. The inertance of the semi-active inerter is equivalent to a base value and an adjustable value, which generates adjustable inertial force F_b. The damping of the semi-active damper is also equivalent to a base value and an adjustable value, which generates adjustable damping force F_c. Adjustable inertial force F_b and adjustable damping force F_c form adjustable force F. The combined adjustable force F is generated by the semi-active inerter and semi-active damper, which does not introduce additional energy to the system so that it is semi-active. The semi-active inerter-based suspended device is shown in Fig. 2.

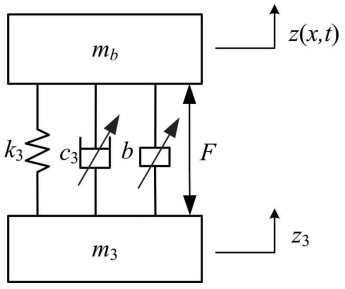

Fig. 2. Semi-active inerter-based suspended device

The dynamic equations of the semi-active coupling dynamic model are given by:

$$\begin{cases} m_b z_b'' = P_1 + P_2 + P_3 + F, \\ I_b \theta_b''(t) = P_1\left(\frac{L}{2} - l_1\right) + P_2\left(\frac{L}{2} - l_2\right) + (P_3 + F)\left(\frac{L}{2} - l_3\right), \\ q_3''(t) + 2\xi_3\omega_3 q_3'(t) + \omega_3^2 q_3(t) = \frac{Y_3(l_1)}{mb}P_1 + \frac{Y_3(l_2)}{mb}P_2 \\ \quad + \frac{Y_3(l_3)}{mb}(P_3 + F), \\ q_4''(t) + 2\xi_4\omega_4 q_4'(t) + \omega_4^2 q_4(t) = \frac{Y_4(l_1)}{mb}P_1 + \frac{Y_4(l_2)}{mb}P_2 \\ \quad + \frac{Y_4(l_3)}{mb}(P_3 + F), \\ m_t z_1'' + c_p(2z_1' - z_{\omega 1}' - z_{\omega 2}') + k_p(2z_1 - z_{\omega 1} - z_{\omega 2}) = -P_1, \\ I_t\theta_1'' + 2l_w^2 c_p\theta_1' + 2l_w^2 k_p\theta_1 = -l_w c_p z_{\omega 1}' + l_w c_p z_{\omega 2}' \\ \quad - l_w k_p z_{\omega 1} + l_w k_p z_{\omega 2}, \\ m_t z_2'' + c_p(2z_2' - z_{\omega 3}' - z_{\omega 4}') + k_p(2z_2 - z_{\omega 3} - z_{\omega 4}) = -P_2, \\ I_t\theta_2'' + 2l_w^2 c_p\theta_2' + 2l_w^2 k_p\theta_2 = -l_w c_p z_{\omega 3}' + l_w c_p z_{\omega 4}' \\ \quad - l_w k_p z_{\omega 3} + l_w k_p z_{\omega 4}, \\ m_3 z_3'' - k_3[z(l_3,t) - z_3] - c_3[z'(l_3,t) - z_3'] \\ \quad - b[z''(l_3,t) - z_3''] = F, \end{cases} \tag{23}$$

where adjustable force F is included in equation (23). Equation (23) could be further expressed as a state form:

$$\mathbf{X}' = \mathbf{A}\mathbf{X} + \mathbf{B}\mathbf{U} + \mathbf{B}_2\mathbf{Z}_\omega, \tag{24}$$

where $\mathbf{A}$ is the system matrix, $\mathbf{B}$ is the input matrix, $\mathbf{B}_2$ is the coefficient matrix of the input track irregularity, $\mathbf{X}$ is the state vector and $\mathbf{U}$ is the control vector. These matrices are given by:

$$\begin{aligned} &\mathbf{X} = [\mathbf{Z} \quad \mathbf{Z}']^T, \quad \mathbf{A} = \begin{bmatrix} \mathbf{0}_{9*9} & \mathbf{I}_{9*9} \\ -\mathbf{M}^{-1}\mathbf{K} & -\mathbf{M}^{-1}\mathbf{C} \end{bmatrix}, \\ &\mathbf{B}_1 = \begin{bmatrix} 1 & 0 & \frac{Y_3(l_3)}{mb} & \frac{Y_4(l_3)}{mb} & 0 & 0 & 0 & 0 & -1 \end{bmatrix}^T, \\ &\mathbf{B} = \begin{bmatrix} \mathbf{0}_{9*1} & -\mathbf{M}^{-1}\mathbf{B}_1 \end{bmatrix}^T, \quad \mathbf{U} = [F], \\ &\mathbf{B}_2 = \begin{bmatrix} \mathbf{0}_{9*1} & \mathbf{M}^{-1}\mathbf{D} \end{bmatrix}^T, \end{aligned} \tag{25}$$

where $\mathbf{Z}_\omega$ is the excitation disturbance vector of the track irregularity and it is shown in equation (17) in Section 2. As self-density $S_{FF}(\omega)$ is obtained, combining equations (18), (25) and (A4), input excitation $\mathbf{B}_2\,\mathbf{Z}_\omega$ in equation (24) can be determined.

The LQR control strategy is applied to adjustable force F. Its object is a linear system expressed in the state space form, the objective function is a quadratic function of the object state and control variable. By designing the state feedback controller $\overline{\mathbf{K}}$, the quadratic objective function J could acquire the minimum value. The controller $\overline{\mathbf{K}}$ is particularly defined by the weight matrix $\mathbf{Q}$ and $\mathbf{R}$, which shows the importance of the choice for $\mathbf{Q}$ and $\mathbf{R}$. The LQR control strategy could acquire optimal control for a linear state feedback system, which constitutes closed-loop optimal control.

The output vector of the controlled system is:

$$\mathbf{y} = \begin{bmatrix} z_b'' & \theta_b'' & z_3'' \end{bmatrix}^T, \tag{26}$$

where $z_b''(x)$, $\theta_b''(x)$ and $z_3''(x)$ are the vertical vibration acceleration of the train body, pitching acceleration of the train body and the vertical vibration acceleration of the underframe suspended device, respectively.

Output vector $\mathbf{y}$ can be determined by the following matrix, which is given as:

$$\begin{aligned} &\mathbf{y} = \mathbf{C}_y\mathbf{X} + \mathbf{D}_y\mathbf{U}, \\ &\mathbf{G} = \begin{bmatrix} 1 & 0 & 0 & 0 & 0 & 0 & 0 & 0 & 0 \\ 0 & 1 & 0 & 0 & 0 & 0 & 0 & 0 & 0 \\ 0 & 0 & 0 & 0 & 0 & 0 & 0 & 0 & 1 \end{bmatrix}, \\ &\mathbf{C}_y = \begin{bmatrix} -\mathbf{G}\mathbf{M}^{-1}\mathbf{K}_1 & -\mathbf{G}\mathbf{M}^{-1}\mathbf{C} \end{bmatrix}, \\ &\mathbf{D}_y = \begin{bmatrix} \mathbf{0}_{3*1} & \mathbf{G}\mathbf{M}^{-1}\mathbf{B}_1 \end{bmatrix}, \end{aligned} \tag{27}$$

where $\mathbf{C}_y$ and $\mathbf{D}_y$ are the output and direct transfer matrices, respectively, and both matrices are constant matrices.

The goal of the LQR control strategy is to find the control vector to minimize the performance index, which is given by:

$$J = \lim_{T\to\infty}\frac{1}{T}E\int_0^\infty \left[q_1 z_b''^2 + q_2\theta_b''^2 + q_3 z_3''^2\right]\mathrm{d}t, \tag{28}$$

while the standard quadratic form of the performance index function J is:

$$J = \lim_{T\to\infty}\frac{1}{T}E\left[\int_0^\infty \left(\mathbf{y}^T\mathbf{Q}\mathbf{y} + \mathbf{U}^T\mathbf{R}\mathbf{U}\right)\mathrm{d}t\right], \tag{29}$$

where $\mathbf{Q}$ and $\mathbf{R}$ are the weighting matrices of the state and control variables, respectively. $\mathbf{Q}$ is a non-negative definite matrix and $\mathbf{R}$ is a positive definite matrix, which is given as:

$$\mathbf{Q} = \mathbf{C}_y^T\mathbf{Q}_0\mathbf{C}_y, \quad \mathbf{R} = \mathbf{D}_y^T\mathbf{Q}_0\mathbf{D}_y, \quad \mathbf{Q}_0 = \begin{bmatrix} q_1 & 0 & 0 \\ 0 & q_2 & 0 \\ 0 & 0 & q_3 \end{bmatrix}. \tag{30}$$

After determining the system parameter values, controller characteristic parameters and weighting coefficients, the optimal feedback gain matrix could be acquired by solving the Riccati equation and is given as:

$$\mathbf{PA}+\mathbf{A}^T\mathbf{P}-\mathbf{PBR}^{-1}\mathbf{B}^T\mathbf{P}+\mathbf{Q}=\mathbf{0}, \tag{31}$$

then the symmetric positive definite matrix $\mathbf{P}$ is obtained and optimal feedback gain matrix $\overline{\mathbf{K}}$ is given by:

$$\overline{\mathbf{K}}=\mathbf{R}^{-1}\mathbf{B}^T\mathbf{P}, \tag{32}$$

where feedback gain matrix $\overline{\mathbf{K}}$ is an N dimensional coefficient matrix, which can be obtained by using the LQR function in MATLAB. Based on the acquired optimal feedback gain matrix $\overline{\mathbf{K}}$ and feedback state variable $\mathbf{X}$, adjustable force F can be obtained:

$$F=-\overline{\mathbf{K}}\mathbf{X}, \tag{33}$$

where $\mathbf{X}$ can be obtained using equation (25) and it equals $[z_b\ \theta_b\ q_3\ q_4\ z_1\ \theta_1\ z_2\ \theta_2\ z_3\ z_b'\ \theta_b'\ q_3'\ q_4'\ z_1'\ \theta_1'\ z_2'\ \theta_2'\ z_3']^T$. The optimal feedback gain matrix equals $[k_1\ k_2\ \cdots\ k_{18}]$.

In the actual control system design, the output needs to be controlled, and the controllability matrix of the control system is expressed as:

$$V_c=\left[\mathbf{C}_y\mathbf{B}\quad \mathbf{C}_y\mathbf{AB}\quad \ldots\quad \mathbf{C}_y\mathbf{A}^{n-1}\mathbf{B}\right], \tag{34}$$

The controllability of the system depends on the rank of controllability matrix $\mathbf{V}_c$, if the rank equals the number of output variables, the system is controllable, which is given as:

$$rank\mathbf{V}_c=rank\left[\mathbf{C}_y\mathbf{B}\quad \mathbf{C}_y\mathbf{AB}\quad \ldots\quad \mathbf{C}_y\mathbf{A}^{n-1}\mathbf{B}\right]=n, \tag{35}$$

combining equations (25) and (27), using the structural parameters of the high-speed train shown in Table 1, the rank of controllability matrix $\mathbf{V}_c$ equals 3, which also equals the number of output variables, and then the system is controllable.

According to the Lyapunov stability theorem, there exists a quadratic Lyapunov function $V(\mathbf{X})=\mathbf{X}^T\mathbf{PX}$ about the symmetric positive definite matrix $\mathbf{P}$ shown in equation (31). Differentiating function $V(\mathbf{X})$ with respect to the time t yields:

$$\begin{aligned}\frac{\mathrm{d}V(\mathbf{X})}{\mathrm{d}t}&=\mathbf{X}^T\mathbf{PX}'+\mathbf{X}'^T\mathbf{PX}\\&=\mathbf{X}^T\left[\mathbf{P}(\mathbf{A}-\mathbf{BR}^{-1}\mathbf{B}^T\mathbf{P})+(\mathbf{A}-\mathbf{BR}^{-1}\mathbf{B}^T\mathbf{P})^T\mathbf{P}\right]\mathbf{X}\\&=\mathbf{X}^T\left[\mathbf{PA}-\mathbf{PBR}^{-1}\mathbf{B}^T\mathbf{P}+\mathbf{A}^T\mathbf{P}-\mathbf{PBR}^{-1}\mathbf{B}^T\mathbf{P}\right]\mathbf{X}\\&=-\mathbf{X}^T[\mathbf{Q}+\mathbf{PBR}^{-1}\mathbf{B}^T\mathbf{P}]\mathbf{X}<\mathbf{0}.\end{aligned} \tag{36}$$

Thus it can be proved that the control system is stable.

In the LQR control strategy, the design of performance index function J is the most important and crucial part, which determines the quality of the control effect. The dynamic response is obtained using MATLAB/Simulink and the weighting coefficient matrix $\mathbf{Q}_0$ is optimized by the particle swarm algorithm. The optimization objective function of the particle swarm algorithm is defined as:

$$L=\frac{\mathrm{RMS}[z_b''(x)]}{\mathrm{RMS}[z_{bp}'']}+\frac{\mathrm{RMS}[\theta_b''(x)]}{\mathrm{RMS}[\theta_{bp}'']}+\frac{\mathrm{RMS}[z_3''(x)]}{\mathrm{RMS}[z_{3p}'']}, \tag{37}$$

where RMS denotes the root mean square value. The denominator denotes the variables using the passive inerter-based suspended device, the numerator denotes the variables using the semi-active inerter-based suspended device. If the optimization objective function L obtains the minimum value, the particle swarm algorithm stops. The optimization process of the weighting coefficient is shown in Fig. 3.

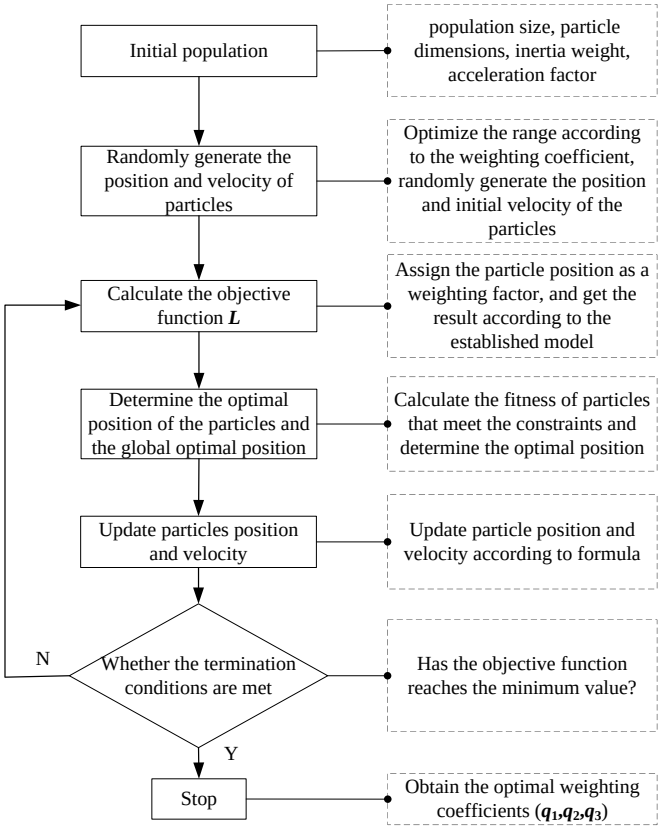

Fig. 3. Optimization process of weighting coefficient using particle swarm algorithm

For the semi-active inerter-based suspended device, the inertance of the semi-active inerter and the damping of the semi-active damper are equivalent to a base value and an adjustable value, and the base values of the semi-active inerter and semi-active damper are chosen as 2080 kg and 8000 N·s/m, respectively. In addition, the stiffness of the spring is chosen as 160798N/m. Bear in mind that the structural parameters of the passive inerter-based suspended device are chosen as the same values that make the optimization objective function a minimum value. The ranges of the weighting coefficients (q_1, q_2, q_3) are from 1×10^{-6} to 1×10^{6}, and they are determined using the particle swarm algorithm to minimize the performance index function J. The setting parameters of the particle swarm

Table 2
Weighting coefficients for the semi-active inerter-based suspended device with different speeds

Weighting coefficient	Speed (km/h)					
	200	230	260	290	320	350
q_1	1×10^{-6}	1×10^{-6}	3.8552×10^{5}	8.9998×10^{5}	4.8230×10^{5}	9.9971×10^{5}
q_2	5.8941×10^{4}	1×10^{6}	9.9986×10^{5}	1×10^{6}	8.1902×10^{5}	1×10^{6}
q_3	1×10^{-6}	1×10^{-6}	3.6232×10^{4}	6.1877×10^{4}	2.5334×10^{4}	3.0070×10^{4}

algorithm are as follows: the population size is set as 80, the maximum number of iterations is set as 300, the particle dimensions are the number of weighting coefficients which equals 3, the range of the initial inertia weight is from 0.4 to 0.9, the range of the acceleration factor is from 0 to 4. Different initial inertia weight and acceleration factors lead to different optimization results. Comparing the optimization results repeatedly and choosing the minimum optimization objective function L as the final result, the initial inertia weight is chosen as 0.58 and the acceleration factor is chosen as 1.52. The weighting coefficients with different speeds are displayed in Table 2.

After determining the weighting coefficients (q_1, q_2, q_3) using the particle swarm algorithm, the weighting coefficient matrix $\mathbf{Q}_0$ could be obtained, then the matrices $\mathbf{Q}$ and $\mathbf{R}$ are obtained based on equations (27) and (30). Through solving the Riccati equation in equation (31) and after combining it with equation (33), the optimal control force can be obtained:

$$F = \mathbf{R}^{-1}\mathbf{B}^{T}\mathbf{P}\mathbf{X}. \tag{38}$$

Using the structural parameters of the high-speed train shown in Table 1, when the speed equals 200 km/h and 350 km/h, respectively, the corresponding feedback gain matrix $\overline{\mathbf{K}}$ is obtained based on equation (32) and is shown in the Appendix, while the corresponding adjustable force F equals 2870N and 2.1×10^{4} N, respectively. Because adjustable force F increases as the speed increases, when the speed of the high-speed train increases from 200 km/h to 350 km/h, the range of adjustable force F is [2870 N, 2.1×10^{4} N]. The base values of the semi-active inerter and semi-active damper are chosen as 2080 kg and 8000 N·s/m, respectively. In addition, for an inerter with a mass of 33 kg, the generated maximum inertance can be 1×10^{4} kg [40]. So adjustable force F can be realized by the semi-active inerter and semi-active damper.

Bear in mind that in practical engineering, the weighting coefficients (q_1, q_2, q_3) are calculated according to the set road conditions and stored in a database. Therefore, in the actual use of the controller, the required weighting coefficients can be obtained by searching the database based on the actual road conditions.

4. DYNAMIC PERFORMANCE ANALYSIS

Typical structural parameters of the high-speed train are adopted and the low interference power spectrum is chosen as the track spectrum for the high-speed train [41], which is given as:

$$S_V(\Omega) = \frac{A_V\Omega_c^2}{(\Omega^2+\Omega_r^2)+(\Omega^2+\Omega_c^2)}, \tag{39}$$

where Ω is the spatial frequency, and Ω_c and Ω_r are the truncated wave numbers and chosen as 0.8246 rad/m and 0.0206 rad/m, respectively. A_v is the roughness coefficient of railway irregularity and chosen as 4.032×10^{-7} m·rad.

The relationship between time frequency ω and space frequency Ω is:

$$\Omega = \omega/v. \tag{40}$$

Furthermore, converting the spatial frequency spectrum of rail irregularities shown in equation (38) into time frequency spectrum yields the following:

$$S_{FF}(\omega) = \frac{2\pi A_v\Omega_c^2 v^3}{[\omega^2+v^2\Omega_r^2]^2+[\omega^2+v^2\Omega_c^2]^2}. \tag{41}$$

The low interference track spectrum is taken as the input excitation, substituting adjustable force F of the semi-active inerter-based suspended device regulated by the LQR control into equation (24) to acquire the dynamic response of the coupling dynamic system.

The vertical vibration acceleration studied in this paper is taken in the middle of the train body, and the changing tendency of its RMS value with different speed is displayed in Fig. 4a, where four different suspended devices are shown in the same figure for comparison, and the thorough values are exhibited in Table 3. The four suspended devices are passive and semi-active traditional suspended devices as well as passive and semi-active inerter-based suspended devices. The traditional suspended device is based on the spring-damper vibration attenuation structure, the stiffness of the spring is chosen as 1 500 000 N/m and the damping of the damper is chosen as 100 000 N·s/m, respectively, which makes objective function J a minimum value. The semi-active traditional suspended device denotes that the damper is semi-active and the LQR control strategy is adopted to adjust the adjustable damping force, while the base value of the semi-active damper is chosen as 100 000 N·s/m, and the resulting weighting coefficients with different speed are displayed in Table 4. The optimization range of the RMS value of the vertical vibration acceleration of the train body using the semi-active traditional, passive and semi-active inerter-based suspended devices compared with the pas-

sive traditional one is shown in Fig. 4b, which is defined as:

$$[\mathrm{RMS}(z_b'')_{\mathrm{PT}} - \mathrm{RMS}(z_b'')_{\mathrm{SAT,PIB,SAIB}}]/\mathrm{RMS}(z_b'')_{\mathrm{PT}} \times 100\%,$$

where the subscript PT, SAT, PIB, SAIB refers to the passive traditional, semi-active traditional, passive and semi-active inerter-based suspended devices, respectively. If the value of the optimization range is the largest, the corresponding suspended device is most beneficial.

As shown in Fig. 4a, when the speed increases, the RMS value of vertical vibration acceleration of the train body using the four suspended devices first decreases and then increases. The RMS value of vertical vibration acceleration of the train body using the passive inerter-based suspended device is smaller than that of the passive traditional one, which indicates the advantages of introducing an inerter. The difference decreases by increasing the speed, which decreases from 18.31% at 200 km/h to 2.65% at 350 km/h. The RMS value of vertical vibration acceleration of the train body using the semi-active inerter-based suspended device is smaller than that of the passive one, which suggests the necessity of using the LQR control strategy, and the differences are obvious as speed increases. In addition, the RMS value of vertical vibration acceleration of the train body using the semi-active inerter-based suspended device is smaller than that of the semi-active traditional one (see Table 3), which further shows the benefits of the inerter. As shown in Fig. 4(b), compared with the passive traditional suspended device, the optimization range of RMS value of vertical vibration acceleration of the train body using the semi-active inerter-based one is the best among the latter three suspended devices, which is most beneficial.

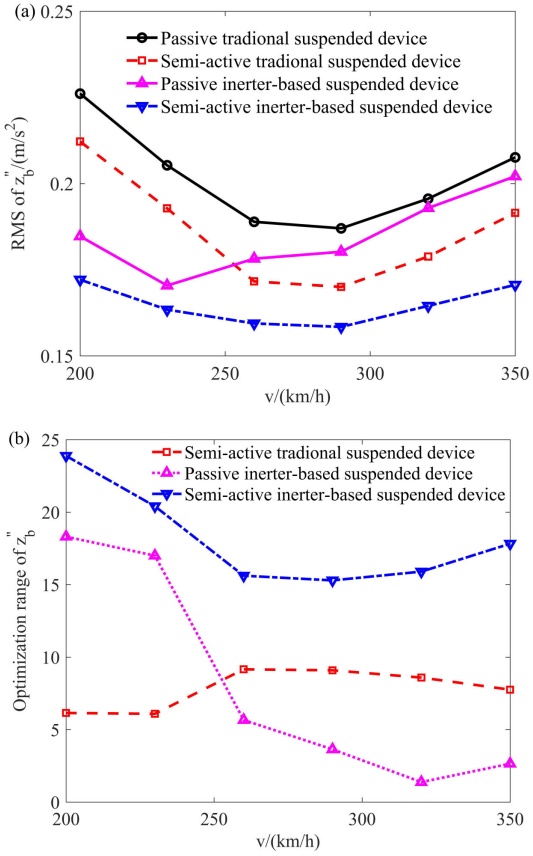

Fig. 4. (a) RMS value of vertical vibration acceleration for four suspended devices, (b) optimization range of the RMS value of vertical vibration acceleration using the latter three suspended devices compared with the passive traditional one

Overall, the RMS value of vertical vibration acceleration of the train body using the semi-active inerter-based suspended device is the smallest among the four suspended devices, and its optimization range as compared with the passive traditional one is more obvious, especially in the lower and higher speed ranges.

In order to clearly show the advantages of the semi-active inerter-based suspended device, the power spectrum density (PSD) of the vertical vibration acceleration of the train body for four suspended devices is shown in Fig. 5, with the running speeds chosen as 200 km/h and 350 km/h, which is elaborated in the aspect of frequency domain. The semi-active inerter-based suspended device could reduce vertical vibration acceleration and further attenuate elastic vibration of the train body significantly in the lower frequency band as compared with the other three suspended devices, while it has little effect in the higher frequency band.

The time domain and frequency domain responses of the vertical vibration acceleration for four suspended devices with two speed are shown in Figs. 6 and 7, respectively. In the time domain, the vertical vibration acceleration of the train body using the semi-active inerter-based suspended device is the smallest among the four suspended devices; In the frequency domain, the resonance peaks for the semi-active inerter-based suspended device is also the smallest among the four suspended devices, which is consistent with the results shown in Figs. 4 and 5.

Table 3
Thorough RMS value of vertical vibration acceleration for four suspended devices

RMS of z_b'' (m/s^2)	Speed (km/h)					
	200	230	260	290	320	350
Passive traditional suspended device	0.2261	0.2053	0.1889	0.1870	0.1956	0.2076
Semi-active traditional suspended device	0.2122	0.1928	0.1716	0.1700	0.1788	0.1915
Passive inerter-based suspended device	0.1847	0.1704	0.1782	0.1802	0.1929	0.2021
Semi-active inerter-based suspended device	**0.1721**	**0.1634**	**0.1594**	**0.1584**	**0.1645**	**0.1706**

Table 4
Weighting coefficients for the semi-active traditional suspended device with different speeds

Weighting coefficient	Speed (km/h)					
	200	230	260	290	320	350
q_1	1×10^{-6}	1×10^{-6}	1×10^{-6}	1×10^{-6}	1×10^{-6}	1×10^{-6}
q_2	1×10^{6}	1×10^{6}	1×10^{-6}	1×10^{-6}	1×10^{-6}	1×10^{-6}
q_3	3.2153	23.4131	117.0833	55.2893	30.0229	20.7305

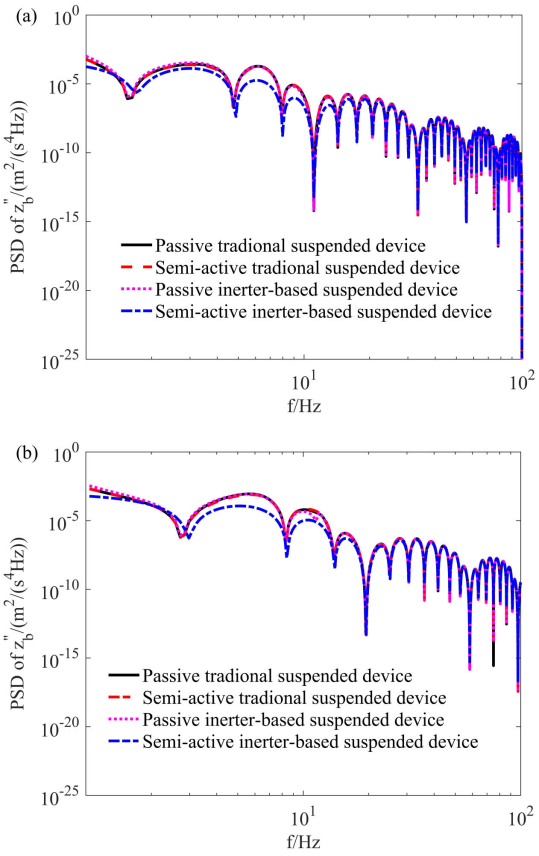

Fig. 5. PSD of vertical vibration acceleration for four suspended devices: (a) $v = 200$ km/h, (b) $v = 350$ km/h

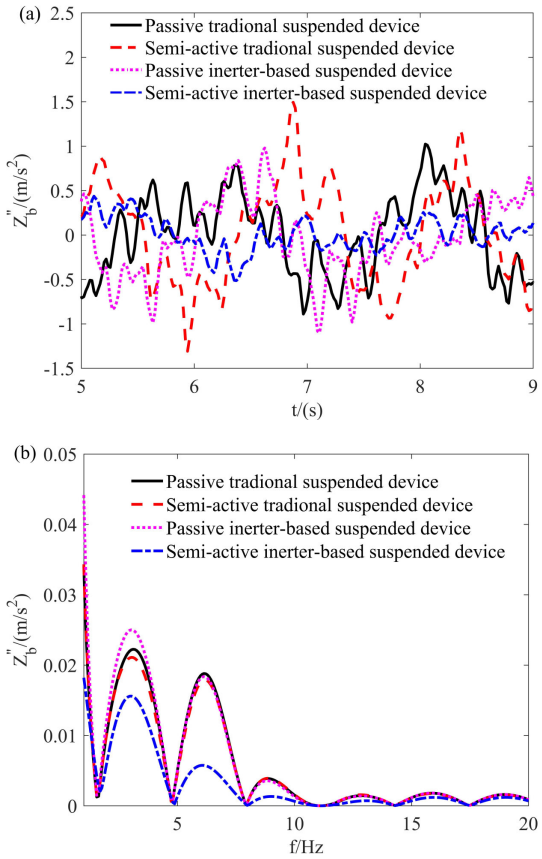

Fig. 6. (a) Time domain and (b) frequency domain responses of vertical vibration acceleration for four suspended devices with $v = 200$ km/h

Furthermore, displacement transmissibility of the train body for four suspended devices is shown in Fig. 8, which is defined as the ratio between displacement in the middle of the train body z_b and input displacement $z_{\omega 1}$. Two main resonance frequencies are observed, and the smaller one corresponds to rigid body vibration while the larger one corresponds to elastic body vibration. The lower resonance peak of displacement transmissibility using four suspended devices remains almost the same, while the higher resonance peak of displacement transmissibility using the semi-active inerter-based suspended device is the smallest among the four ones. This further clarifies the reason for the corresponding vertical vibration acceleration to be the smallest, as shown in Fig. 4 and Table 3.

The Sperling index [39] is used to evaluate running quality of the high-speed train. The smaller the Sperling index, the better the running quality of the train. The Sperling index at each excitation frequency can be obtained as:

$$W_k = 2.7 \cdot \sqrt[10]{a_k f_k^5 F(f_k)} = 0.896 \cdot \sqrt[10]{a_k F(f_k)/f_k}, \tag{42}$$

where f_k is the excitation frequency, a_k is the acceleration amplitude for f_k, and $F(f_k)$ is the weighting coefficient related to the excitation frequency, and it is given by:

$$F(f_k) = \begin{cases} 0.325 f_k^2 & 0.5 < f_k \le 5.9, \\ \dfrac{400}{f_k^2} & 5.9 < f_k \le 20, \\ 1 & f_k > 20. \end{cases} \tag{43}$$

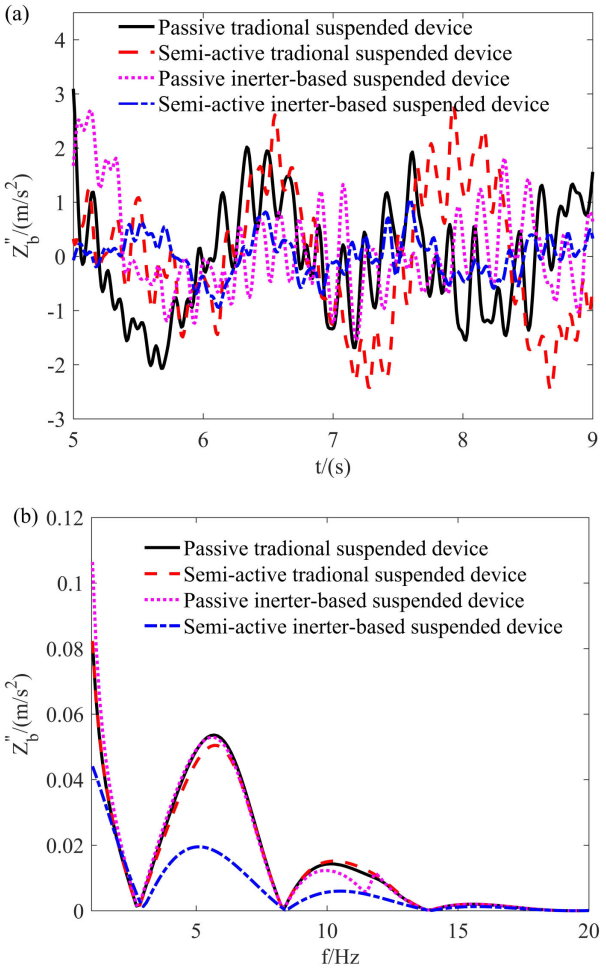

Fig. 7. (a) Time domain and (b) frequency domain responses of vertical vibration acceleration for four suspended devices with $v = 350$ km/h

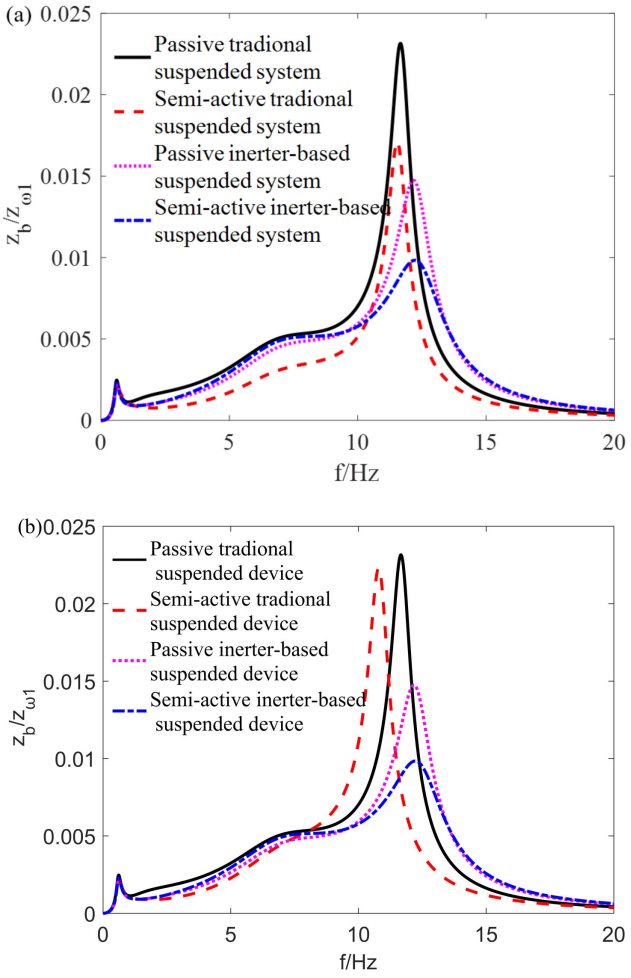

Fig. 8. Displacement transmissibility of train body for four suspended devices: (a) $v = 200$ km/h, (b) $v = 350$ km/h

The Sperling index for each excitation frequency could be obtained and the total Sperling indexes in the excitation frequency band are given as:

$$W_{\text{tot}} = \sqrt[10]{(W_1^{10} + \cdots + W_n^{10})}. \tag{44}$$

Furthermore, based on equations (22), (42), (43) and (44), the Sperling index could be obtained. For a high-speed train, the Sperling index is divided into three grades [42], which is excellent when it is smaller than 2.5, good when it is between 2.5 and 2.75, and qualified when it is between 2.75 and 3.

The Sperling index is also taken in the middle of the train body and its changing tendency for four suspended devices with different speed is displayed in Fig. 9(a), while detailed values are shown in Table 5. The optimization range of the Sperling index using the semi-active traditional, passive and semi-active inerter-based suspended devices as compared with the passive traditional one is shown in Fig. 9(b), which is defined as [(Sperling index)$_{PT}$–(Sperling index)$_{SAT,PIB,SAIB}$]/(Sperling index)$_{PT} \times 100\%$. If the value of the optimization range is the largest, the corresponding suspended device obtains the best running quality.

As shown in Fig. 9(a), the Sperling index for four suspended devices shows an overall upward tendency via increasing the speed, and is smaller than 2.5, with all of them achieving an excellent effect. The Sperling index of the passive inerter-based suspended device is smaller than the passive traditional one, and the corresponding difference between the passive inerter-based and traditional ones experiences an overall upward tendency through increasing the speed, which increases from 2.28% at 200 km/h to 10.4% at 350 km/h. The Sperling index of the semi-active inerter-based suspended device is smaller than that of the passive one, and the difference is smaller in the lower and medium speed ranges while it increases in the larger speed ranges. Furthermore, the Sperling index of the semi-active inerter-based suspended device is generally smaller than that of the semi-active traditional one. As shown in Fig. 9(b), as compared with the passive traditional suspended device, the optimization range of Sperling index using the semi-active inerter-based one is the best among the latter three suspended devices, and it obtains the best running quality.

In general, the Sperling index of the semi-active inerter-based suspended device is the smallest among the four suspended devices. The semi-active inerter-based suspended device could

Table 5
Thorough value of Sperling index for four suspended devices

Sperling index	Speed (km/h)					
	200	230	260	290	320	350
Passive traditional suspended device	1.8830	2.0044	2.2797	2.1948	2.1948	2.3400
Semi-active traditional suspended device	1.8608	1.9119	1.8669	1.9004	1.9691	2.0380
Passive inerter-based suspended device	1.8400	1.8341	1.8868	1.9687	2.0418	2.0967
Semi-active inerter-based suspended device	**1.8357**	**1.8155**	**1.8393**	**1.8923**	**1.9598**	**2.0133**

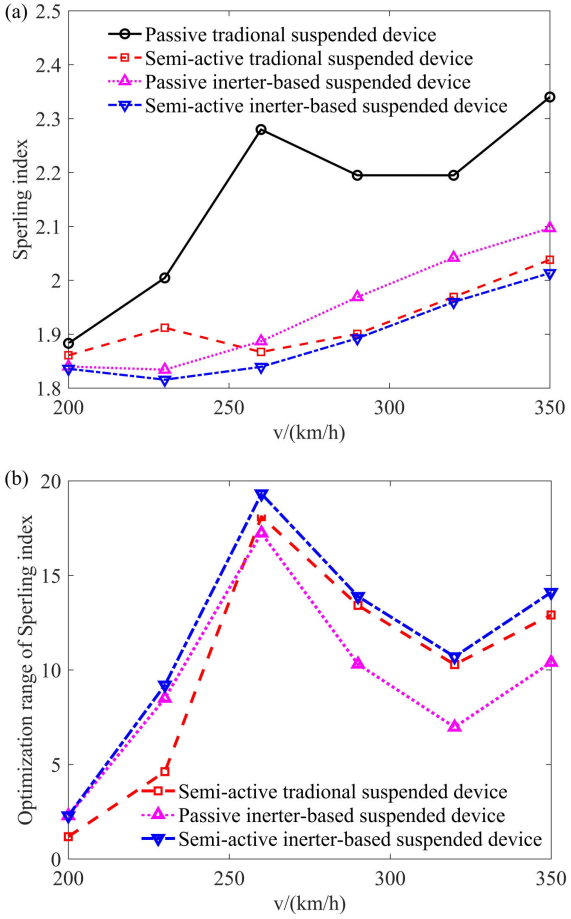

Fig. 9. (a) Sperling index for four suspended devices, (b) optimization range of Sperling index using the latter three suspended devices compared with the passive traditional one

significantly reduce elastic vibration of the train body. The more severe the elastic vibration, the more obvious the vibration attenuation effect of the train body, which is consistent with the results of the vertical vibration acceleration shown in Figs. 4 and 5.

5. CONCLUSIONS

A semi-active inerter-based suspended device based on the semi-active inerter and damper is proposed to further enhance dynamic performance of the train body. The LQR control strategy is utilized to adjust the inertance of the semi-active inerter and the damping of the semi-active damper. The rigid-flexible coupling vertical dynamic model of the train body and semi-active inerter-based suspended device is established, dynamic response is obtained using the virtual excitation method, and the dynamic characteristic is evaluated using the Sperling index and compared with those of the other suspended devices. The conclusions are summarized as follows:

1. The vertical vibration acceleration of the train body using the semi-active inerter-based suspended device is the smallest among the four suspended devices, which denotes the advantages of using the inerter and LQR control strategy.
2. The semi-active inerter-based suspended device could decrease the vertical vibration acceleration of the train body and further suppress its elastic vibration significantly in the lower frequency band as compared with the other three ones, while it has little effect in the higher frequency band.
3. The Sperling index of the semi-active inerter-based suspended device is generally the smallest among the four suspended devices, and the vibration attenuation effect is more obvious for more severe elastic vibration.

Overall, the semi-active inerter-based suspended device is a novel design and could further decrease elastic vibration of the train body and improve the dynamic performance more effectively than the other three suspended devices.

APPENDIX

Mass matrix $\mathbf{M}$, damping matrix $\mathbf{C}$, stiffness matrix $\mathbf{K}_1$ and input excitation matrix $\mathbf{D}$ defined in equation (9) are given as:

$$\mathbf{M} = \begin{bmatrix} m_b+b & 0 & bY_3(l_3) & bY_4(l_3) & 0 & 0 & 0 & 0 & -b \\ 0 & I_b & 0 & 0 & 0 & 0 & 0 & 0 & 0 \\ b/m_b & 0 & 1+b/m_b & 0 & 0 & 0 & 0 & 0 & -b/m_b \\ 0 & 0 & 0 & 1 & 0 & 0 & 0 & 0 & 0 \\ 0 & 0 & 0 & 0 & m_t & 0 & 0 & 0 & 0 \\ 0 & 0 & 0 & 0 & 0 & I_t & 0 & 0 & 0 \\ 0 & 0 & 0 & 0 & 0 & 0 & m_t & 0 & 0 \\ 0 & 0 & 0 & 0 & 0 & 0 & 0 & I_t & 0 \\ -b & 0 & -bY_3(l_3) & bY_4(l_3) & 0 & 0 & 0 & 0 & m_3+b \end{bmatrix}, \quad \text{(A1)}$$

$$\mathbf{C} = \begin{bmatrix} 2c_s + c_3 & 0 & (Y_3(l_1) + Y_3(l_2))c_s + Y_3(l_3)c_3 \\ 0 & 2c_s l_b^2 & (Y_3(l_1) - Y_3(l_2))c_s l_b \\ \dfrac{(Y_3(l_1) + Y_3(l_2))c_s + y_{33}c_3}{m_b} & \dfrac{(Y_3(l_1) - Y_3(l_2))c_s l_b}{m_b} & \dfrac{(Y_3(l_1)^2 + Y_3(l_2)^2)c_s + c_3 y_{33}^2}{m_b} + 2x_3 w_3 \\ \dfrac{(Y_3(l_1) + Y_3(l_2))c_s + y_{33}c_3}{m_b} & \dfrac{(Y_3(l_1) - Y_3(l_2))c_s l_b}{m_b} & \dfrac{(c_s Y_3(l_1)Y_4(l_1) + c_s Y_4(l_2)Y_3(l_2) + c_3 Y_3(l_3)Y_4(l_3))}{m_b} \\ -c_s & -c_s l_b & -Y_3(l_1)c_s \\ 0 & 0 & 0 \\ -c_s & c_s l_b & -Y_4(l_1)c_s \\ 0 & 0 & 0 \\ -c_s & 0 & -Y_3(l_3)c_3 \end{bmatrix}$$

$$\begin{bmatrix} (Y_4(l_1) + Y_4(l_2))c_s + Y_4(l_3)c_3 & -c_s & 0 & -c_s & 0 & -c_3 \\ (Y_4(l_1) - Y_4(l_2))c_s l_b & -c_s l_b & 0 & c_s l_b & 0 & 0 \\ \dfrac{c_s Y_3(l_1)Y_4(l_1) + c_s Y_4(l_2)Y_3(l_2) + c_3 Y_3(l_3)Y_4(l_3)}{m_b} & -\dfrac{c_s Y_3(l_1)}{m_b} & 0 & -\dfrac{c_s Y_3(l_2)}{m_b} & 0 & -\dfrac{c_3 Y_3(l_3)}{m_b} \\ \dfrac{(Y_4(l_1)^2 + Y_4(l_2)^2)c_s + Y_4(l_3)^2 c_3}{m_b} + 2x_4 w_4 & -\dfrac{c_s Y_4(l_1)}{m_b} & 0 & -\dfrac{c_s Y_4(l_2)}{m_b} & 0 & -\dfrac{c_3 Y_4(l_3)}{m_b} \\ -Y_3(l_2)c_s & -\dfrac{c_s Y_3(l_1)}{m_b} & 0 & 0 & 0 & 0 \\ 0 & 0 & 2c_p l_w^2 & 0 & 0 & 0 \\ -Y_4(l_2)c_s & 0 & 0 & 2c_p l_w^2 & 0 & 0 \\ 0 & 0 & 0 & 0 & 2c_p l_w^2 & 0 \\ -Y_4(l_3)c_3 & 0 & 0 & 0 & 0 & c_3 \end{bmatrix}, \tag{A2}$$

$$\mathbf{K}_1 = \begin{bmatrix} 2k_s + k_3 & 0 & (Y_3(l_1) + Y_3(l_2))k_s + Y_3(l_3)k_3 \\ 0 & 2k_s l_b^2 & (Y_3(l_1) - Y_3(l_2))k_s l_b \\ \dfrac{(Y_3(l_1) + Y_3(l_2))k_s + Y_3(l_3)k_3}{m_b} & \dfrac{(Y_3(l_1) - Y_3(l_2))k_s l_b}{m_b} & \dfrac{(y_{31}^2 + y_{32}^2)k_s + k_3 Y_3(l_3)^2}{m_b} + 2w_3^2 \\ \dfrac{(Y_3(l_1) + Y_3(l_2))k_s + Y_3(l_3)k_3}{m_b} & \dfrac{(Y_3(l_1) - Y_3(l_2))k_s l_b}{m_b} & \dfrac{(c_s Y_3(l_1)Y_4(l_1) + c_s Y_4(l_2)Y_3(l_2) + c_3 Y_3(l_3)Y_4(l_3))}{m_b} \\ -k_s & -k_s l_b & -Y_3(l_1)k_s \\ 0 & 0 & 0 \\ -k_s & k_s l_b & -Y_4(l_1)c_s \\ 0 & 0 & 0 \\ -k_s & 0 & -Y_3(l_3)k_3 \end{bmatrix}$$

$$\begin{bmatrix} (Y_4(l_1) + Y_4(l_2))k_s + Y_4(l_3)k_3 & -k_s & 0 & -k_s & 0 & -k_3 \\ (Y_4(l_1) - Y_4(l_2))k_s l_b & -k_s l_b & 0 & k_s l_b & 0 & 0 \\ \dfrac{k_s Y_3(l_1)Y_4(l_1) + k_s Y_4(l_2)Y_3(l_2) + k_3 Y_3(l_3)Y_4(l_3)}{m_b} & -\dfrac{k_s Y_3(l_1)}{m_b} & 0 & -\dfrac{k_s Y_3(l_2)}{m_b} & 0 & -\dfrac{k_3 Y_3(l_3)}{m_b} \\ \dfrac{(Y_4(l_1)^2 + Y_4(l_2)^2)k_s + Y_4(l_3)^2 k_3}{m_b} + 2w_4^2 & -\dfrac{k_s Y_4(l_1)}{m_b} & 0 & -\dfrac{k_s Y_4(l_2)}{m_b} & 0 & -\dfrac{k_3 Y_4(l_3)}{m_b} \\ -Y_3(l_2)k_s & k_s + 2k_p & 0 & 0 & 0 & 0 \\ 0 & 0 & 2k_p l_w^2 & 0 & 0 & 0 \\ -Y_4(l_2)k_s & 0 & 0 & k_s + 2k_p & 0 & 0 \\ 0 & 0 & 0 & 0 & 2k_p l_w^2 & 0 \\ -Y_4(l_3)k_3 & 0 & 0 & 0 & 0 & k_3 \end{bmatrix}, \tag{A3}$$

$$\mathbf{D} = \begin{bmatrix} 0 & 0 & 0 & 0 & 0 & 0 & 0 & 0 \\ 0 & 0 & 0 & 0 & 0 & 0 & 0 & 0 \\ 0 & 0 & 0 & 0 & 0 & 0 & 0 & 0 \\ 0 & 0 & 0 & 0 & 0 & 0 & 0 & 0 \\ k_p & c_p & k_p & c_p & 0 & 0 & 0 & 0 \\ -k_p l_w & -c_p l_w & k_p l_w & c_p l_w & 0 & 0 & 0 & 0 \\ 0 & 0 & 0 & 0 & k_p & c_p & k_p & c_p \\ 0 & 0 & 0 & 0 & -k_p l_w & -c_p l_w & k_p l_w & c_p l_w \\ 0 & 0 & 0 & 0 & 0 & 0 & 0 & 0 \\ 0 & 0 & 0 & 0 & 0 & 0 & 0 & 0 \end{bmatrix}. \quad \text{(A4)}$$

When the speed equals 200 km/h and 350 km/h, respectively, the corresponding feedback gain matrix $\overline{\mathbf{K}}$ is obtained based on equation (32), and is equal to:

$$\overline{\mathbf{K}} = \begin{bmatrix} 1438508 \\ -773.052 \\ -1.5 \times 10^{7} \\ 201785.5 \\ 34142.71 \\ -2.16 \times 10^{-11} \\ 38972.66 \\ -3.58 \times 10^{-11} \\ -1412863 \\ 60975.23 \\ -1447.76 \\ -115020 \\ 228.8301 \\ 1550.385 \\ -5.06 \times 10^{-13} \\ -651.536 \\ -2.86 \times 10^{-12} \\ -58097.8 \end{bmatrix}^T, \quad \overline{\mathbf{K}} = \begin{bmatrix} -339416 \\ -20.10 \\ 2321958 \\ 22692 \\ -7845.81 \\ 5.46 \times 10^{-13} \\ -9317.41 \\ -1.32 \times 10^{-12} \\ 66604.88 \\ -53674.12 \\ 89.61 \\ 172432.21 \\ 60.58 \\ -2439.07 \\ 2.21 \times 10^{-15} \\ -2454.62 \\ -8.29 \times 10^{-15} \\ 31107.24 \end{bmatrix}^T. \quad \text{(A5)}$$

ACKNOWLEDGEMENTS

This work was supported by the National Natural Science Foundation of China (Grant No. 12172153, 51805216), State Key Laboratory of Automotive Simulation and Control (Jilin University) (Grant No. 20210212), Key Laboratory of Road and Traffic Engineering of the Ministry of Education (Tongji University) (Grant No. K202005), the Major Project of Basic Science (Natural Science) of the Jiangsu Higher Education Institutions (22KJA410001) and the project funded by the Youth Talent Cultivation Program of Jiangsu University.

REFERENCES

[1] F. Ripamonti and A. Chiarabaglio, "A smart solution for improving ride comfort in high-speed railway vehicles," *J. Vib. Control*, vol. 25, no. 13, pp. 1958–1973, 2019, doi: 10.1177/1077546319843377.

[2] J. Wu and Y. Qiu, "Analysis of ride comfort of high-speed train based on a train-seat-human model in the vertical direction," *Veh. Syst. Dyn.*, vol. 59, pp. 1867–1893, 2021, doi: 10.1080/00423114.2020.1794014.

[3] J.F. Sun, M.R. Chi, W.B. Cai, and H.X. Gao, "An investigation into evaluation methods for ride comfort of railway vehicles in the case of carbody hunting instability," *Proc Inst. Mech. Eng. F J. Rail Rapid Transit*, vol. 235, no. 5, pp. 586–597, 2021, doi: 10.1177/0954409720949116.

[4] Q.S. Wang, J. Zeng, L. Wei, and B. Zhu, "Carbody vibrations of high-speed train caused by dynamic unbalance of underframe suspended equipment," *Adv. Mech. Eng.*, vol. 10, no. 12, pp. 1–13, 2018, doi: 10.1177/1687814018818969.

[5] M. Dumitriu M, "A new passive approach to reducing the carbody vertical bending vibration of railway vehicles," *Veh. Syst. Dyn.*, vol. 55, no. 11, pp. 1787–1806, 2017, doi: 10.1080/00423114.2017.1330962.

[6] T. Tomioka and T. Takigami, "Reduction of bending vibration in railway vehicle carbodies using carbody-bogie dynamic interaction," *Veh. Syst. Dyn.*, vol. 48, no. 5, pp. 467–486, 2010, doi: 10.1080/00423114.2010.490589.

[7] D. Gong, J.S. Zhou, and W.J. Sun, "Influence of under-chassis-suspended equipment on high-speed EMU trains and the design of suspension parameters," *Proc. Inst. Mech. Eng. F J. Rail Rapid Transit*, vol. 230, no. 8, pp. 1790–1802, 2016, doi: 10.1177/0954409715614601.

[8] S. Yang, F. Li, H.L. Shi, and P.B. Wu, "A roll frequency design method for underframe equipment of a high-speed railway vehicle for elastic vibration reduction," *Veh. Syst. Dyn.*, 2021, doi: 10.1080/00423114.2021.1899252.

[9] M.C. Smith, "Synthesis of mechanical networks: the inerter," *IEEE Trans. Autom. Control*, vol. 47, no. 10, pp. 1648–1662, 2002, doi: 10.1109/CDC.2002.1184758.

[10] Y. Wang, H. Ding, and L.Q. Chen, "Averaging analysis on a semi-active inerter-based suspension system with relative-acceleration-relative-velocity control," *J. Vib. Control*, vol. 26, no. 13–14, pp. 1199–1215, 2020, doi: 10.1177_1077546319891612.

[11] L. Yang, R.C. Wang, X.P. Meng, Z.Y. Sun, W. Liu, and Y. Wang, "Performance analysis of a new hydropneumatic inerter-based suspension system with semi-active control effect," *Proc. Inst. Mech. Eng. D J. Automob. Eng.*, vol. 234, no. 7, pp. 1883–1896, 2020, doi: 10.1177/0954407019894189.

[12] Y.C. Zeng, H. Ding, R.H. Du, and L.Q. Chen, "A suspension system with quasi-zero stiffness characteristics and inerter nonlinear energy sink," *J. Vib. Control*, vol. 28, pp. 143–158, 2022, doi: 10.1177/1077546320972904.

[13] Y. Li, J.Z. Jiang, S.A. Neild, and H.L. Wang, "Optimal inerter-based shock-strut configurations for landing-gear touchdown performance," *J. Aircr.*, vol. 54, no. 5, pp. 1901–1909, 2017, doi: 10.2514/1.C034276.

[14] S.Y. Zhang, J.Z. Jiang, and S.A. Neild, "Optimal configurations for a linear vibration suppression device in a multi-storey building," *Struct. Control Health Monit.*, vol. 24, no. 3, pp. 1–17, 2017, doi: 10.1002/stc.1887.

[15] Z.P. Zhao, R.F. Zhang, Y.Y. Jiang, and C. Pan, "Seismic response mitigation of structures with a friction pendulum inerter system," *Eng. Struct.*, vol. 193, pp. 110–120, 2019, doi: 10.1016/j.engstruct.2019.05.024.

[16] Y. Hu and M.Z.Q. Chen, "Performance evaluation for inerter-based dynamic vibration absorbers," *Int. J. Mech. Sci.*, vol. 99, pp. 297–307, 2015, doi: 10.1016/j.ijmecsci.2015.06.003.

[17] Y. Wang, H.X. Li, C. Cheng, H. Ding, and L.Q. Chen, "Dynamic performance analysis of a mixed-connected inerter-based quasi-zero stiffness vibration isolator," *Struct. Control Health Monit.*, vol. 27, no. 10, pp. e2604, 2020, doi: 10.1002/stc.2604.

[18] Y. Wang, H.X. Li, C. Cheng, H. Ding, and L.Q. Chen, "A nonlinear stiffness and nonlinear inertial vibration isolator," *J. Vib. Control*, vol. 27, no. 11-12, pp. 1336–1352, 2021, doi: 10.1177/1077546320940924.

[19] Y. Wang, H.D. Meng, B.Y. Zhang, and R.C. Wang, "Analytical research on the dynamic performance of semi-active inerter-based vibration isolator with acceleration-velocity-based control strategy," *Struct. Control Health Monit.*, vol. 26, no. 4, pp. e2336, 2019, doi: 10.1002/stc.2336.

[20] J.Z. Jiang, Z.M.S. Alejandra, M.G. Roger, and M.C. Smith, "Passive suspensions incorporating inerters for railway vehicles," *Veh. Syst. Dyn.*, vol. 50, pp. 263–276, 2012, doi: 10.1080/00423114.2012.665166.

[21] H.J. Chen, W.J. Su, and F.C. Wang, "Modeling and analyses of a connected multi-car train system employing the inerter," *Adv. Mech. Eng.*, vol. 9, no. 8, pp. 1–13, 2017, doi: 10.1177/1687814017701703.

[22] T.D. Lewis, J.Z. Jiang, S.A. Neild, C. Gong, and S.D. Iwnicki, "Using an inerter-based suspension to improve both passenger comfort and track wear in railway vehicles," *Veh. Syst. Dyn.*, vol. 58, no. 3, pp. 472–493, 2020, doi: 10.1080/00423114.2019.1589535.

[23] Y. Wang, H.X. Li, W.A. Jiang, R.C. Wang, and Y. Li, "Dynamic characteristics of underframe inerter-based suspended equipment for high speed train," *J. Vib. Shock*, vol. 41, no. 2, pp. 251–259, 2022, (in Chinese). [Online] Available: http://jvs.sjtu.edu.cn/EN/Y2022/V41/I2/246.

[24] L. Peng, J. Wang, G. Yu, G.C. Yu, and Z.X. Wang, "Active Vibration Control of PID Based on Receptance Method," *J. Sensors*, vol. 2, pp. 1–8, 2020, doi: 10.1155/2020/8811448.

[25] B.K. Cho, G Ryu, and S.J. Song, "Control strategy of an active suspension for a half car model with preview information," *Int. J. Autom. Technol.*, vol. 6, no. 3, pp. 234–249, 2005. [Online] Available: https://www.koreascience.or.kr/article/JAKO200502637296964.pdf.

[26] M.M. Michalek, "Robust trajectory following without availability of the reference time-derivatives in the control scheme with active disturbance rejection," in *American Control Conference IEEE*, 2016, doi: 10.1109/ACC.2016.7525134.

[27] K. Akomy and M.M. Michalek, "Robust output-feedback VFO-ADR control of underactuated spatial vehicles in the task of following non-parametrized paths," *Eur. J. Control*, 2020, doi: 10.1016/j.ejcon.2020.07.006.

[28] Y. Peng and S.Z. Yang, "The connection between discrete and continuous state constrained optimal control systems," *Int. J. Control Autom. Syst.*, vol. 94, no. 9, pp. 2337–2344, 2019, doi: 10.1080/00207179.2019.1706765.

[29] L. Fu, Y. Ma, and C.J. Wang, "Memory sliding mode control for semi-Markov jump system with quantization via singular system strategy," *Int. J. Robust Nonlinear Control*, vol. 29, no. 18, pp. 6555–6571, 2019, doi: 10.1002/rnc.4735.

[30] H. Zhang, H.Y. Dong, B.P. Zhang, "Research on beam supply control strategy based on sliding mode control," *Arch. Electr. Eng.*, vol. 69, no. 2, pp. 349–364, 2020, doi: 10.24425/aee.2020.133030.

[31] X. Wang, B. Xu, S. Li, "Composite Learning Fuzzy Control of Stochastic Nonlinear Strict-Feedback Systems," *IEEE Trans. Fuzzy Syst.*, vol. 29, no. 4, pp. 705–715, 2021, doi: 10.1109/TFUZZ.2019.2960736.

[32] Y. Zhu, H. Zhao, H. Sun, S. Zhen, and Z. Zhu, "Robust control design of electric helicopter tail reduction system: fuzzy and optimal view," *J. Vib. Control*, vol. 26, no. 9–10, pp. 814–829, 2020, doi: 10.1177/1077546319889852.

[33] S.M.M. Bideleh, T.X. Mei, and V. Berbyuk, "Robust control and actuator dynamics compensation for railway vehicles," *Veh. Syst. Dyn.*, vol. 54, no. 10, pp. 1762–1784, 2016, doi: 10.1080/00423114.2016.1234627.

[34] A. Daraghmeh and N. Qatanani, "Numerical error bound of optimal control for homogeneous linear systems," *Arch. Gerontol. Geriat.*, vol. 29, no. 2, pp. 323–337, 2019, doi: 10.24425/acs.2019.129385.

[35] Y.C. Zeng, W.H. Zhang, and D.L. Song, "Lateral-vertical coupled active suspension on railway vehicle and optimal control methods," *Veh. Syst. Dyn.*, vol. 60, pp. 258–280, 2022, doi: 10.1080/00423114.2020.1814358.

[36] L. Yulianti, A. Nazra, Zulakmal, A. Bahar, and Muhafzan, "On discounted LQR control problem for disturbanced singular system," *Arch. Control Sci.*, vol. 29, no. 1, pp. 147–156, 2019, doi: 10.24425/acs.2019.127528.

[37] Q.S. Wang, J. Zeng, Y. Wu, and B. Zhu, "Study on semi-active suspension applied on carbody underneath suspended system of high-speed railway vehicle," *J. Vib. Control*, vol. 26, no. 9-10, pp. 671–679, 2020, doi: 10.1177/1077546319889863.

[38] W.J. Sun, J.S. Zhou, D. Thompson, and D. Gong, "Vertical random vibration analysis of vehicle-track coupled system using Green's function method," *Veh. Syst. Dyn.*, vol. 52, no. 3, pp. 362–389, 2014, doi: 10.1080/00423114.2014.884227.

[39] C.H. Huang, J. Zeng, G.B. Luo, and H.L. Shi, "Numerical and experimental studies on the car body flexible vibration reduction due to the effect of car body-mounted equipment," *Proc. Inst. Mech. Eng. F J. Rail Rapid Transit*, vol. 232, no. 1, pp. 103–120, 2018, doi: 10.1177/0954409716657372.

[40] T.A. Stachiw, F. Khouli, R.G. Langlois, and F.F. Afagh, "The Use of an Inerter in an Aircraft Landing Gear Suspension for Improved Passenger and Crew Comfort at Touchdown," *AIAA Scitech 2020 Forum*, doi: 10.2514/6.2020-1681.

[41] C.X. Deng, J.S. Zhou, D. Thompson, D. Gong, W.J. Sun, and Y. Sun, "Analysis of the consistency of the sperling index for rail vehicles based on different algorithms," *Veh. Syst. Dyn.*, vol. 59, no. 2, pp. 313–330, 2021, doi: 10.1080/00423114.2019.1677923.

[42] D. Gong, J.S. Zhou, and W.J. Sun, "On the resonant vibration of a flexible railway car body and its suppression with a dynamic vibration absorber," *J. Vib. Control*, vol. 19, no. 5, pp. 649–657, 2013, doi: 10.1177/1077546312437435.